

This is a repository copy of *The application of extreme ultra-violet lasers in plasma heating and diagnosis*.

White Rose Research Online URL for this paper:

<https://eprints.whiterose.ac.uk/102843/>

Version: Accepted Version

---

**Proceedings Paper:**

Tallents, Greg J. [orcid.org/0000-0002-1409-105X](https://orcid.org/0000-0002-1409-105X), Aslanyan, Valentin, Rossall, Andrew [orcid.org/0000-0002-0123-8163](https://orcid.org/0000-0002-0123-8163) et al. (2 more authors) (2015) The application of extreme ultra-violet lasers in plasma heating and diagnosis. In: Proceedings of SPIE - The International Society for Optical Engineering. X-Ray Lasers and Coherent X-Ray Sources: Development and Applications XI Conference, 12-13 Aug 2015 SPIE , USA

<https://doi.org/10.1117/12.2187986>

---

**Reuse**

Items deposited in White Rose Research Online are protected by copyright, with all rights reserved unless indicated otherwise. They may be downloaded and/or printed for private study, or other acts as permitted by national copyright laws. The publisher or other rights holders may allow further reproduction and re-use of the full text version. This is indicated by the licence information on the White Rose Research Online record for the item.

**Takedown**

If you consider content in White Rose Research Online to be in breach of UK law, please notify us by emailing [eprints@whiterose.ac.uk](mailto:eprints@whiterose.ac.uk) including the URL of the record and the reason for the withdrawal request.

# The application of extreme ultra-violet lasers in plasma heating and diagnosis

Greg. J Tallents\*, Valentin Aslanyan, Andrew Rossall, Sarah Wilson and Mohammed Shahzad  
York Plasma Institute, Department of Physics, University of York, York YO10 5DD, U.K.

## ABSTRACT

Laser-plasma studies have been undertaken for 50 years using infra-red to ultra-violet lasers. We show that a new regime of laser-produced plasmas can be created with capillary discharge and free electron lasers operating in the extreme ultra-violet (EUV). For example, EUV radiation (wavelength  $< 50$  nm) has a critical electron density above electron densities formed by ionization at solid material density and so potentially can penetrate to large depth into a solid density plasma. We explore here the importance of this penetration in ablating solid targets, in creating novel warm dense matter and in the diagnosis of plasmas.

**Keywords:** Extreme ultra-violet, plasma, ablation, warm dense matter.

## 1. INTRODUCTION

When a visible or infra-red high power laser pulse is focused onto a solid target, the first photons in the leading edge of the pulse produce free electrons by multi-photon processes, with the bulk of the laser energy interacting with plasma expanding normally to the target surface. Consequently, laser light only penetrates through the expanding plasma plume up to a critical density, which is typically a factor  $10^{-2} - 10^{-3}$  less than the solid density. Dropping the laser wavelength  $\lambda$  into the extreme ultra-violet (EUV) (to  $\lambda < 50$  nm) causes the critical density to be greater than the electron density produced at solid density. The laser light can now interact through a solid target over an attenuation length defined by the level of photo-ionization. The enhanced penetration of EUV laser radiation enables laser-plasmas in the warm dense regime to be created and also serves to enable the diagnosis of optical laser-produced plasmas by probing.

## 2. EUV LASER ABLATION

For basic research and to enable the development of industrial applications, there is a need to produce compact and affordable extreme ultra-violet (EUV) and x-ray laser sources for use in parallel with large-scale free-electron laser facilities such as FLASH<sup>1</sup>. Capillary lasers have been demonstrated to be useful pulsed energy sources of coherent EUV laser radiation. For example, a table-top-size soft-x-ray laser system based upon capillary discharge excitation of an Ar gas produces lasing at 46.9 nm with a pulse energy up to 0.8 mJ and a pulse length of 1.2 ns (see Benware et al<sup>2</sup>). We have used a combination of fluid code modeling with atomic physics to simulate such EUV and similarly soft x-ray interaction when focused with irradiances  $> 10^9$  Wcm<sup>-2</sup> onto a solid. Our code POLLUX models the laser energy deposition within the target, thermal energy transport, and the subsequent ablative flow away from the target. We have adapted a 2D hydrodynamic code originally written by Pert<sup>3</sup> to simulate optical and infrared-laser interaction by adding new absorption and atomic physics to enable the simulation of the ablation of solids by EUV and x-ray lasers. A more detailed study of EUV laser ablation is presented in this proceedings by Rossall et al<sup>4</sup> and only a brief over-view is given in this paper.

To calculate bound-free absorption processes within the target material in EUV interactions with solids, a model of atomic structure is used to account for transitions from both the ground and excited states. As the produced plasma is close to solid density, the ionization energy is lowered due to the presence of the surrounding electrons and ions. This ionization potential depression can cause pressure ionization, thus, reducing the absorption of the laser in that region. Ion potential depression is accounted for using the model developed by Stewart and Pyatt (for a recent review of ionization depression models, see Preston et al<sup>5</sup>). Ionic- and excited-state populations are determined by assuming local thermodynamic equilibrium using the Saha-Boltzmann relation. Although the initial plasma state is highly non-

\*greg.tallents@york.ac.uk; phone 44 1904 32 2286; <http://www.york.ac.uk/physics/people/tallents/>

equilibrated, we found that due to the high densities involved, the plasma ionization equilibrates on a time scale of tens of femtoseconds due to electron collisional ionization, excitation and the inverse processes of three-body recombination and collisional de-excitation. The fluid code simulations shown here operate on a hydrodynamic time scale of  $> 1$  ps; enabling a local thermodynamic equilibrium assumption to be valid. An analytical approximation of the Kramers-Kronig relationship is used to determine temperature-dependent atomic scattering factors and, thus, the refractive index of the plasma. Our model for refractive index calculations has been reported previously<sup>6</sup>.

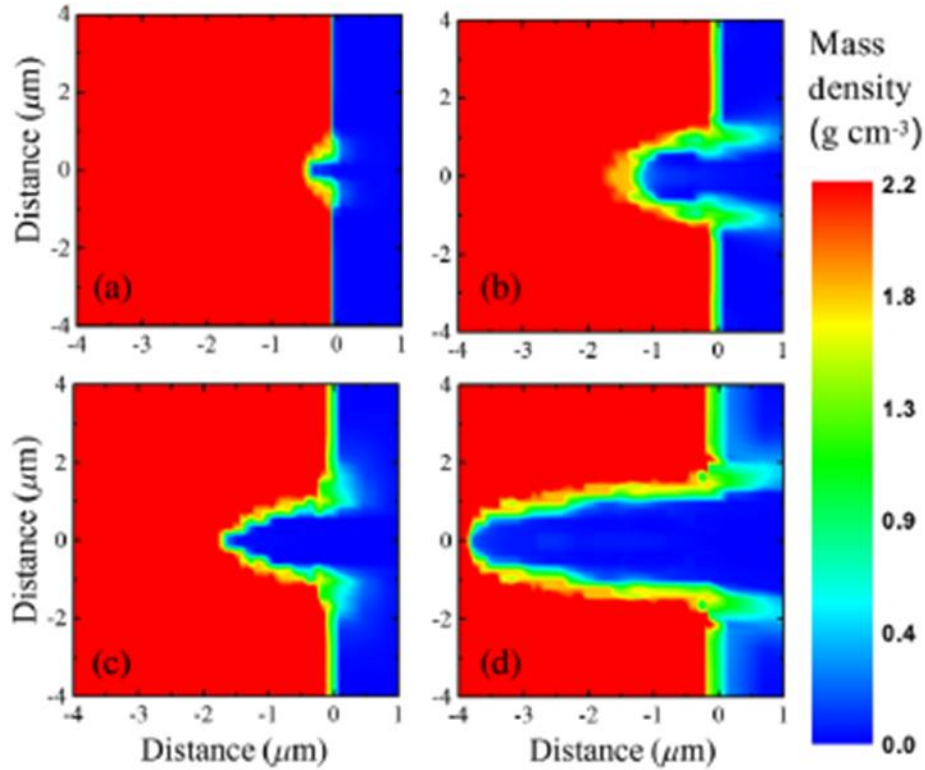


Figure 1. Single shot ablation profiles of craters in parylene-N irradiated by an EUV (wavelength 46.9 nm) laser of 1.3n pulse duration at different peak irradiances (a)  $10^9$   $\text{W cm}^{-2}$ , (b)  $10^{10}$   $\text{W cm}^{-2}$ , (c)  $10^{11}$   $\text{W cm}^{-2}$  and (d)  $10^{12}$   $\text{W cm}^{-2}$ . The focal spot diameter assumed is 500 nm (originally published by Rossall et al<sup>7</sup>).

To explore the ablative capabilities of EUV lasers, the effect of varying the irradiance from  $1 \times 10^9$   $\text{W cm}^{-2}$  to  $1 \times 10^{12}$   $\text{W cm}^{-2}$  has been simulated, the results of which are shown in Fig. 1. Ablated depths of  $3.8 \mu\text{m}$  per pulse are observed for the highest irradiance with a lateral hole size of  $2.2 \mu\text{m}$  (FWHM) for a  $0.5 \mu\text{m}$  diameter (FWHM) focal width. High-aspect-ratio submicron-size surface features are achievable, provided the system is optimized to inhibit lateral heat transport within the target. Figure 1 shows ablation profiles as a function of irradiance after 1300 ps of irradiation and demonstrates that lateral heat transport increases the feature size with increasing fluence as one would expect due to the increase in localized energy deposition in the target. Typical predicted temperatures for the laser-produced plasma range between a few electron volts for an on-target laser irradiance of  $10^9$   $\text{W cm}^{-2}$  to 80 eV for  $10^{12}$   $\text{W cm}^{-2}$  with plasma flow velocities along the laser axis ranging between  $10^5$  and  $10^7$   $\text{cm s}^{-1}$ .

We justify use of the Saha-Boltzmann equation for the calculation of ionization in our POLLUX modelling of EUV laser ablation by the results from two modelling studies. An earlier study<sup>8</sup> has shown that the typical timescales for local thermodynamic equilibrium (LTE) to be achieved is less than 100 fs. We have used scenarios of energy deposition into an initially cold plasma to obtain a density  $1/\rho^2$  scaling law for the time taken by a plasma to reach equilibrium. Such times suggest that the assumption of LTE in many EUV and optical laser plasmas is valid when compared to the hydrodynamic timescales, which occur on timescales of the order of picoseconds. For example, it is appropriate to use LTE as a simplifying assumption for population distributions in models of solid density plasmas heated to electron temperatures less than 100 eV after times of typically 90 fs for iron and 70 fs for carbon (see figure 2).

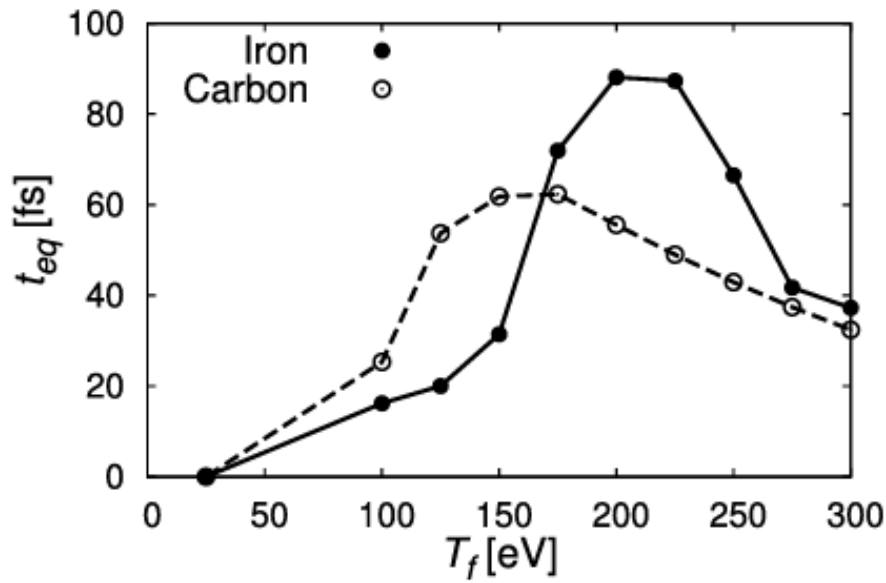


Figure 2. The time to reach an equilibrium population distribution starting with an equilibrium population with electron temperature 25 eV and final temperature as shown on the horizontal axis achieved by linear temperature increase over 100 fs. Results are shown for iron and carbon plasmas at solid iron and graphite densities.

A second study<sup>9</sup> has calculated the effects of assuming that the electron distribution is given by the Fermi-Dirac distribution appropriate where electron degeneracy is high, rather than assuming a Maxwellian distribution of electrons as is usual with collisional-radiative codes. We are dealing with cold, solid density plasmas produced in EUV laser interactions with solids, so the issue of the electron distribution is not clear *a priori* for our POLLUX modelling. Population calculations show insignificant differences to calculations assuming nondegenerate free electrons of plasmas at solid density close to local thermodynamic equilibrium, but show departures in average ionization in the presence of strong EUV photoionization at irradiances  $> 10^{14} \text{ W cm}^{-2}$  (see figure 3).

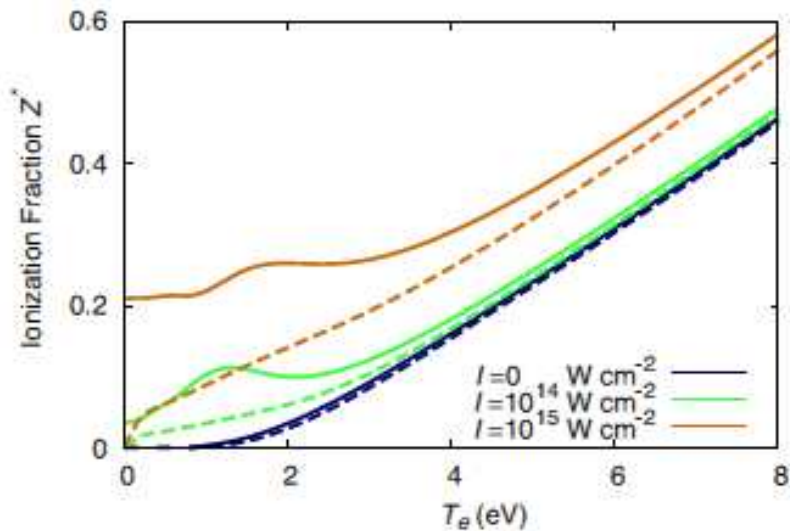


Figure 3. A comparison of the equilibrium ionization with impinging EUV (photon energy 50 eV) laser radiation at the irradiances shown assuming Fermi-Dirac free electron distributions (solid curves) and Maxwellian free electron distributions (broken curves). The curves are a for a carbon plasma at solid graphite density.

### 3. EUV PROBING

Our study reported by Shahzad et al<sup>10</sup> has shown that energy transport to a buried layer of iron in an otherwise plastic target can be evaluated by measuring the transmission of 13.9 nm wavelength (89 eV) EUV transmission through the target. The iron layer becomes transparent when ionized to stages greater than  $Fe^{4+}$  and so transmission becomes a diagnostic of the energy transport into the target. Simulations using the Hyades code with a post-process for the EUV laser opacity are used to compare to experimental transmission measurements (some sample simulation results are shown in figure 4). We have also compared different models of plasma opacity (figure 5). Our work suggests that the opacity of iron at 89 eV for electron temperature 20 eV and  $0.3 \text{ gcm}^{-3}$  is a factor two higher than calculated by some models with a value  $1.1 \times 10^5 \text{ cm}^2 \text{ g}^{-1}$  as suggested in recent work by Bailey et al<sup>11</sup>.

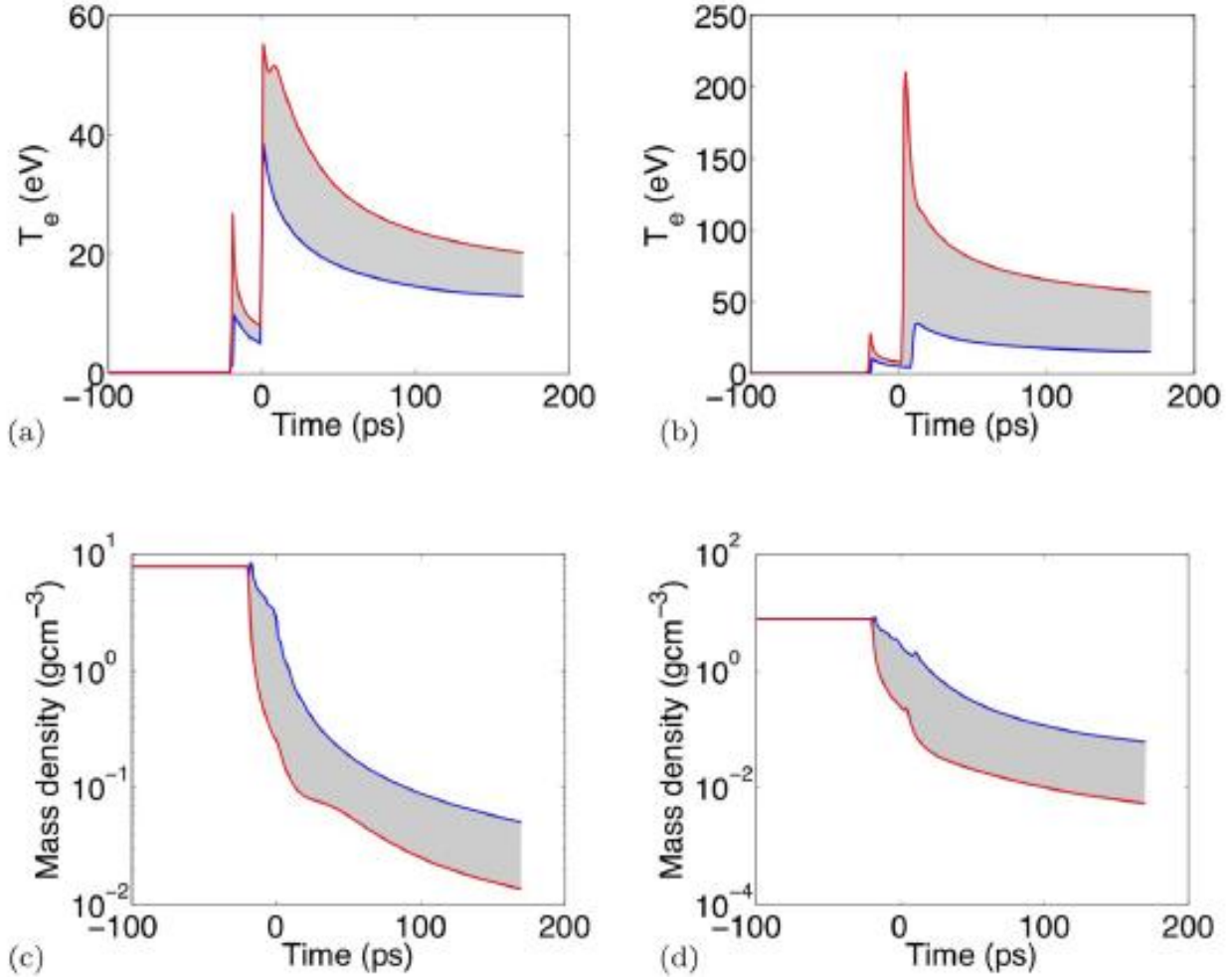


Figure 4. HYADES simulated electron temperatures and densities as a function of time for the initially 50 nm thick iron layer buried beneath 50 nm of parylene-N and irradiated at  $3 \times 10^{16} \text{ Wcm}^{-2}$  with a 35 fs pulse with 10%, 35 fs pre-pulse 20 ps before the main pulse. Plots (a) and (c) are calculated with radiation transport and hot electron heating, while plots (b) and (d) are calculated with radiation transport and hot electron heating turned off.

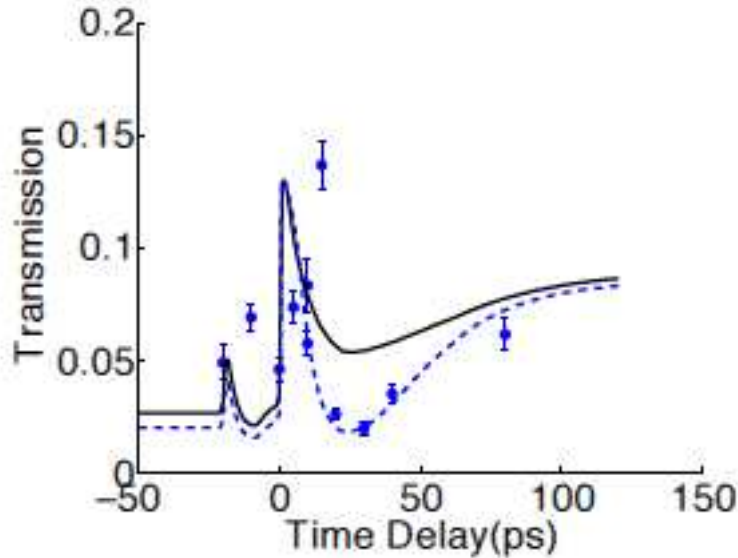


Figure 5. Data points show the measured transmission of 89 eV EUV laser photons through an irradiated target as a function of time. A pre-pulse at -20 ps and peak irradiance  $3 \times 10^{15} \text{ Wcm}^{-2}$  is followed by the main 35 fs pulse at zero time and  $3 \times 10^{16} \text{ Wcm}^{-2}$ . The solid curve is calculated using the HYADES code and a post-processor assuming standard opacity value, while the broken curve assumes an increase of iron opacity.

#### 4. CONCLUSION

We have shown simulation results of ablation due to EUV irradiation of solid plastic targets and some results of probing of a laser-produced plasma with an EUV laser. Narrow deep features can be ablated with EUV lasers as collective effects do not prevent the penetration of radiation as the critical density for EUV wavelengths exceeds the electron density. Similarly, with probing, it is possible to longitudinally probe through buried layer targets in order to record opacity changes in a buried layer of iron due to heat transport into the target.

#### ACKNOWLEDGEMENTS

We acknowledge the U.K. Engineering and Physical Sciences Research Council for grant support to undertake the work reported in this paper. We would like to thank Carmen Menoni, Jorge Rocca and others at Colorado State University for their collaboration on EUV ablation studies and to thank Olivier Guilbaud and others working on the LASERIX facility, Université Paris-Sud for their collaboration on EUV diagnostic probing.

#### REFERENCES

- [1] Tiedtke, K. et al, "The soft x-ray free-electron laser FLASH at DESY: Beamlines, diagnostics and end-stations," *New J. Phys.* 11, 023029 (2009).
- [2] Benware, B. R., Machchietto, C. D., Moreno, C. H. and Rocca, J. J., "Demonstration of a High Average Power Tabletop Soft X-Ray Laser," *Phys. Rev. Lett.* 81, 5804 (1998).
- [3] Pert, G. J., "Two-dimensional hydrodynamic models of laser-produced plasmas," *J. Plasma Phys.* 41, 263 (1989).
- [4] Rossall, A. K., Aslanyan, V., Wilson, S. and Tallents, G. J., "Generation of strongly-coupled plasmas using Argon-based capillary discharge lasers," *Proc. SPIE submitted for publication* (2015).

- [5] Preston, T. R., Vinko, S. M., Ciricosta, O., Chung, H. K., Lee, R. W. and Wark, J. S., "The effects of ionization potential depression on the spectra emitted by hot dense aluminium plasmas," *High Energy Density Phys.* 9, 258 (2013).
- [6] Rossall, A. K. and Tallents, G. J., "Generation of warm dense matter using an argon based capillary discharge laser," *High Energy Density Phys.* 15, 67 (2015).
- [7] Rossall, A. K. et al, "Ablation of Submicrometer Holes Using an Extreme-Ultraviolet Laser," *Phys. Rev. Appl.* 3, 064013 (2015).
- [8] Aslanyan, V. and Tallents, G. J., "Local thermodynamic equilibrium in rapidly heated high energy density plasmas," *Phys. Plasmas* 21, 062702 (2014).
- [9] Aslanyan, V. and Tallents, G. J., "Ionization rate coefficients in warm dense plasmas," *Phys. Rev. E* 91, 063106 (2015).
- [10] Shahzad, M. et al, "Diagnosis of energy transport in iron buried layer targets using an extreme ultraviolet laser," *Phys. Plasmas* 22, 023301 (2015).
- [11] Bailey, J. E., et al, "A higher than predicted measurement of iron opacity at solar interior temperatures," *Nature* 517, 55 (2015).